Neural Network Based Image Modification for Shape from Observed SEM Images

Yuji Iwahori
Dept. of Computer Science
Chubu University
Kasugai 487-8501, Japan
Email: iwahori@cs.chubu.ac.jp

Kenji Funahashi
Dept. of Computer Science
Nagoya Inst. of Tech.
Nagoya 466-8555, Japan
Email: kenji@nitech.ac.jp

Robert J. Woodham
Dept. of Computer Science
Univ. of British Columbia
Canada V6T 1Z4
Email: woodham@cs.ubc.ca

M. K. Bhuyan
Dept. of E.E. Eng.
IIT Guwahati
Guwahati, 781039 India
Email: mkb@iitg.ernet.in

Abstract—A new approach to recover 3-D shape from a Scanning Electron Microscope (SEM) image is described. With an ideal SEM image, 3-D shape can be recovered using the Fast Marching Method (FMM) applied to the Eikonal equation. However, when the light source direction is oblique, the correct shape cannot be obtained by the usual one-pass FMM. The new approach modifies the intensities in the original SEM image using an additional SEM image of a sphere and Neural Network (NN) training. Image modification is a two degree-of-freedom (DOF) rotation. No assumption is made about the specific functional form for intensity in an SEM image. The correct 3-D shape can be obtained using the FMM and NN learning, without iteration. The approach is demonstrated through computer simulation and validated through real experiment.

I. INTRODUCTION

A new approach is described to recover the 3-D shape of an object imaged using a Scanning Electron Microscope (SEM). The approach is based on non-parametric image intensity modification. Related approaches are summarized in the following.

Pentland [1] proposed *Linear Shape from Shading* to recover shape from shading in one image under the assumption that the reflectance function is linear. Pentland [1] uses a light source direction different from the viewpoint (i.e., camera direction) under the assumption that reflectance is approximately linear under wide angle illumination.

Ikeuchi and Horn [2] proposed *Shape from Occluding Boundaries* to recover shape from shading in one image. The approach uses regularization and the resulting algorithm is iterative. Initialization is based on the geometric information at occluding boundaries. On an occluding boundary, surface orientation is orthogonal to both the contour of the boundary and to the 3-D viewing direction. Iterative relaxation combines the initial geometric information at occluding boundaries with interior shading to estimate surface gradient densely. The method works best for simple, closed, convex, curved surfaces.

Other methods recover shape using multiple images of an object under rotation. Laurentini [3] proposed *Shape from Silhouette* that uses multiple images through 360 degrees of rotation. Difficulties arise when the object has local concavities. Shape is determined based on the convex hull of the observed image silhouettes. Accuracy of the obtained result also depends on the step increment in angle between each rotational view. Lu and Little [4] use 90 degrees of rotation of an object. Their method recovers shape from many images obtained during rotation with a small step increment in angle.

With an SEM, there is no equivalent to controlling the angle between the illumination and the viewpoint. Objects imaged with an SEM often have complex shape. Further, the ability to rotate an object being imaged with an SEM is restricted. Consequently, the above approaches cannot be applied directly to SEM images.

Iwahori *et al.* [5] developed Radial Basis Function Neural Network (RBF-NN) photometric stereo. Subsequently, Iwahori *et al.* [6] introduced an optimization based approach that uses two images obtained with rotation of the object stand. Optimization is applied using a Hopfield like Neural Network (HF-NN) [7]. The initial vector determined by the RBF-NN is given to the HF-NN for optimization. Iwahori *et al.* [8] use the FMM to recover 3-D shape. A single, directional light source aligned with the viewing direction is assumed. Non-Lambertian reflectance is handled via self-calibration based on controlled rotation of the target object. Unfortunately, this method also is not directly applicable to SEM images. Stereo vision approaches to SEM images are the exception [9], [10], [11]. The photometric approach of Ding *et al.* [15] uses a single viewpoint. It estimates surface reflectance through rotations of the target object. Tankus *et al.* [14] is another monocular vision approach to recover 3-D shape from a single image. They provide an iterative approach, based on the FMM, applicable to objects with Lambertian reflectance. They also address the problem of an oblique light source. Iteration improves the recovered shape to a degree, as is demonstrated in our comparison experiment. At the same time, our experiments demonstrate that our method produces higher accuracy with relaxed assumptions about the functional form of reflectance and without iteration.

Iwahori *et al.* [16] describe an approach to modify an SEM image based on a synthesized image of a sphere. However, that approach assumed a parametric model for SEM reflectance used for image synthesis. This paper extends that work to make it possible to recover 3-D shape directly. Intensity modification is based on the SEM image of a real calibration sphere. An affine transformation is estimated to align the electron beam and viewing direction. A neural network (NN) is trained with data from the calibration sphere and subsequently used on SEM images of target objects to produce modified images. The FMM is applied to the modified image, without iteration, to recover the 3-D shape of the target object.
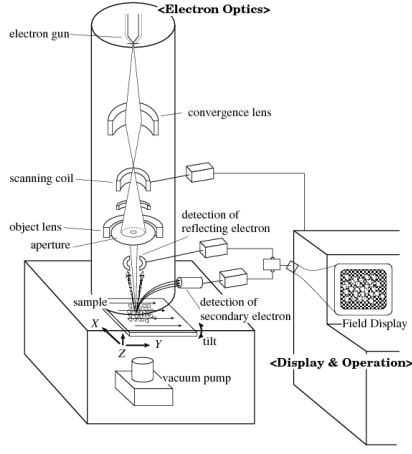
Fig. 1. Scanning Electron Microscope

The remaining sections of the paper review the relevant characteristics of an SEM image, describe the approach used to recover 3-D shape under an oblique light source, and demonstrate the approach through computer simulation and real experiment.

II. CHARACTERISTICS OF AN SEM IMAGE

The relevant architecture and reflectance characteristics of an SEM are summarized. The architecture is shown in Fig. 1. An SEM image has the following properties [2]:

(1) Brightness is lowest for points where the surface normal is toward the viewer.
(2) Light source direction and viewpoint are assumed to be aligned (in the ideal case).
(3) Cast shadow does not occur.

Intensity, $I_{x,y}$, in an SEM image is often represented as

$$I_{x,y} = \frac{I_{min}}{\cos \theta_{x,y}} = I_{min}\sqrt{1 + p_{x,y}^2 + q_{x,y}^2} \qquad (1)$$

where, for each image point (x, y), $\theta_{x,y}$ is the angle between the direction of the electron beam and the surface normal and $(p_{x,y}, q_{x,y})$ is the surface gradient (i.e., p and q are the partial derivatives of z with respect to x and y). I_{min} is the minimum value of observed image intensity, assumed to correspond to a surface normal pointing directly at the electron beam.

This paper relaxes condition (2) to consider the case of an oblique light source. Further, the particular functional form for intensity given in Eq. (1) is not assumed. As a consequence, shape can be recovered with greater accuracy.

III. SHAPE FROM SEM WITH OBLIQUE LIGHT SOURCE

A. Fast Marching Method (FMM) for Lambertian Reflectance

Kimmel and Sethian [13] introduced shape recovery using the FMM [12]. Assumptions made are that the light source direction is aligned with the viewing direction and that reflectance is Lambertian. With these assumptions, the image irradiance equation becomes

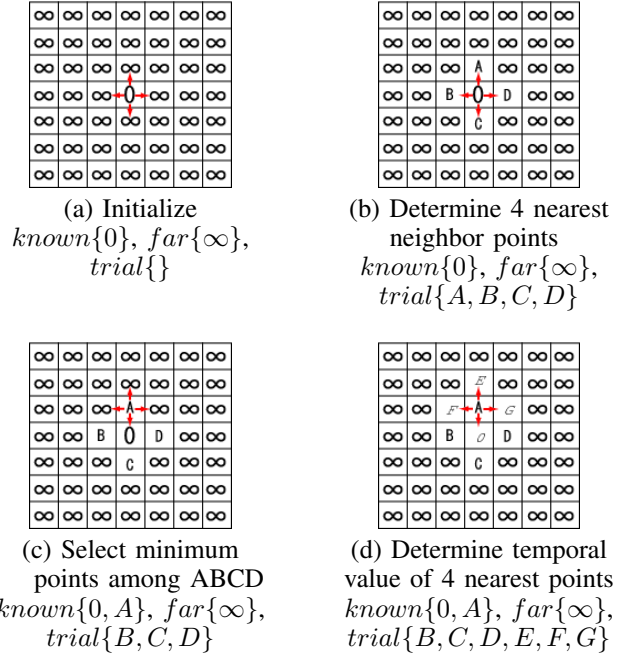$$E = \frac{1}{\sqrt{p^2 + q^2 + 1}} \qquad (2)$$

(a) Initialize
$known\{0\}$, $far\{\infty\}$,
$trial\{\}$

(b) Determine 4 nearest neighbor points
$known\{0\}$, $far\{\infty\}$,
$trial\{A, B, C, D\}$

(c) Select minimum points among ABCD
$known\{0, A\}$, $far\{\infty\}$,
$trial\{B, C, D\}$

(d) Determine temporal value of 4 nearest points
$known\{0, A\}$, $far\{\infty\}$,
$trial\{B, C, D, E, F, G\}$

Fig. 2. FMM

where (p, q) is the surface gradient (i.e., p and q are the partial derivatives of z with respect to x and y). Eq. (2) can be rewritten as

$$\sqrt{p^2 + q^2} = \sqrt{\frac{1}{E^2} - 1} \qquad (3)$$

Eq. (3) is known as the Eikonal equation. The FMM [12] is a fast algorithm to solve the Eikonal equation. Its operation is illustrated in Fig. 2. Being able to formulate shape from shading as a solution to the Eikonal equation allows one to use the FMM to recover object shape from one image. Thus, many approaches assume Lambertian reflectance and light source direction aligned with the viewpoint and use FMM to solve the associated Eikonal equation. These assumptions, however, cannot be applied directly to SEM images.

B. Generation of Modified Image from SEM Image of Sphere

The goal is to transform an actual SEM image into one that would have been obtained had the viewpoint been aligned with the electron beam. The SEM image of a real sphere is used to estimate the required transformation. Suppose an SEM image of a real sphere is acquired under the condition that the apparent viewpoint is not aligned with the electron beam (i.e., the light source is oblique). The physical characteristic of SEM imaging that still holds is that measured intensity is isotropic (i.e., rotationally symmetric) about the light source direction.

Under these conditions, the SEM image of the sphere can be transformed geometrically into one in which intensity is rotationally symmetric about the viewing direction. Suppose the local minimum intensity of the SEM image of the sphere occurs at a point whose surface normal, OP, has zenith angle, α, and azimuth angle, β, with respect to the Z axis, as shown in Fig. 3.

Fig. 3. Angles α and β of the Affine Transformation
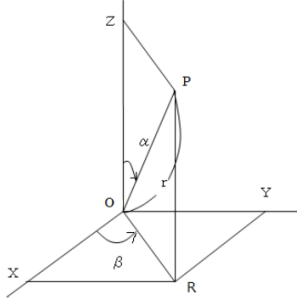
An affine transformation is used to align the vector OP with the Z axis. The transformation is modeled as the following two steps. First, the vector OP is rotated by an angle $-\beta$ about the Z axis. This rotates the vector OP into the XZ plane. Second, the vector is rotated by an angle $-\alpha$ about the Y axis. This aligns the original vector OP with the Z axis. Any other surface normal on the original sphere can be similarly transformed.

The associated affine transformation is first

$$\begin{bmatrix} X' \\ Y' \\ Z' \end{bmatrix} = \begin{bmatrix} \cos(-\beta) & -\sin(-\beta) & 0 \\ \sin(-\beta) & \cos(-\beta) & 0 \\ 0 & 0 & 1 \end{bmatrix} \begin{bmatrix} X \\ Y \\ Z \end{bmatrix} \quad (4)$$

then

$$\begin{bmatrix} X' \\ Y' \\ Z' \end{bmatrix} = \begin{bmatrix} \cos(-\alpha) & 0 & \sin(-\alpha) \\ 0 & 1 & 0 \\ -\sin(-\alpha) & 0 & \cos(-\alpha) \end{bmatrix} \begin{bmatrix} X \\ Y \\ Z \end{bmatrix} \quad (5)$$

The two rotations, Eq. (4) and Eq. (5), are applied to every point on the calibration sphere to produce a modified image of the calibration sphere. Intensity values from the obliquely illuminated calibration sphere are mapped forward to become the intensity values in the modified image. Interpolation is applied to the modified image, as a post process, to fill any small gaps (i.e., any pixels missed) after applying the affine transformation to each point in the original image. This modified image models the image that would have been acquired had the original electron beam been aligned with the viewing direction. This modified image of the calibration sphere is used to train the NN that is used to similarly map the SEM image of a test object of unknown shape, as described in the next subsection.

C. Intensity Modification for Oblique Light Source Image

Depending on the location of the electron detector, SEM images can appear as if obtained with an oblique light source. The goal is to improve the accuracy of previous methods by first producing a modified image corresponding to what would have been obtained with a viewer aligned (i.e., frontal) light source. The intensity modification is performed by nonlinear transformation implemented as a NN. The reason that a NN implementation was chosen is that neural networks are well suited to perform nonparametric function approximation with high accuracy.

The NN is trained with input/output data from the original and modified SEM images of the calibration sphere. The NN

is subsequently used to modify the intensity distribution of the image of a target object.

A Radial Basis Function Neural Network (RBF-NN), as proposed by Chen *et al.* [17], is one choice that has proved suitable in many applications. In particular, it is a choice that has been widely used for strict interpolation tasks in multidimensional spaces. An RBF-NN often can be designed in a fraction of the time it takes to train standard feed-forward networks. An RBF-NN can work well when many training vectors are available. An RBF-NN represents non-linearity via the choice of basis function. The Gaussian is not the only choice of basis function but it is a choice widely used and the one used here.

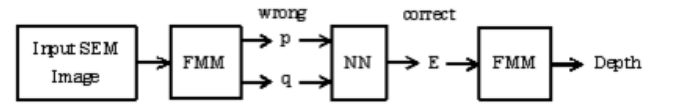The overall intensity modification processing pipeline is shown in Fig. 4.

Fig. 4. Intensity Modification Processing Pipeline

The processing steps are as follows:

(1) FMM is applied to the SEM image of the calibration sphere. This image has a local minimum point and this local minimum is used as the initial point. FMM estimates an initial z distribution.

(2) Surface gradient, (p, q), is determined numerically from the z distribution estimated in step (1). It is expected that these (p, q) values are "wrong" (with an oblique light source). In calibration, surface gradients are used as input to train the required NN. For each given wrong (p, q), the associated output for NN training is the intensity, E, the (p, q) maps to in the modified image of the calibration sphere, as described in the previous subsection. For a test object, intensity at each point is modified to be the output, E, produced by the NN when the wrong (p, q) is given as input.

(3) FMM is applied again to recover a more accurate depth map.

For a test object, FMM is applied in the same way as for the calibration sphere (step (1)). Again, numerical estimation of (p, q) produces "wrong" values (step (2)). These "wrong" values are used as input to the NN trained during calibration to produce a modified image. FMM is applied once again to the modified image (step (3)). Our experiments show that the resulting z distribution is of higher accuracy. Multiple iterations of FMM are not required, in contrast to [14].

D. Obtain $\sqrt{p^2 + q^2}$ from Intensity, E, and Apply FMM

Given the SEM image of a test object, we need to obtain a value for $\sqrt{p^2 + q^2}$ from intensity, E, at each surface point. A conversion table is generated. The estimate of $\sqrt{p^2 + q^2}$ is expressed as a third order polynomial equation in E

$$\sqrt{p^2 + q^2} = aE^3 + bE^2 + cE + d \qquad (6)$$

Estimation is based on the modified calibration sphere image. A linear least square method is used. Suppose there are n points on the quadrant along the equator of the sphere. Then,

$$\begin{bmatrix} E_1^3 & E_1^2 & E_1 & 1 \\ E_2^3 & E_2^2 & E_2 & 1 \\ \vdots & \vdots & \vdots & \vdots \\ E_n^3 & E_n^2 & E_n & 1 \end{bmatrix} \begin{bmatrix} a \\ b \\ c \\ d \end{bmatrix} = \begin{bmatrix} \sqrt{p_1^2 + q_1^2} \\ \sqrt{p_2^2 + q_2^2} \\ \vdots \\ \sqrt{p_n^2 + q_n^2} \end{bmatrix} \qquad (7)$$

Eq. (7) is of the form $\boldsymbol{Ax} = \boldsymbol{y}$. The coefficients $\boldsymbol{x} = [a, b, c, d]^T$ can be determined as $\boldsymbol{x} = (\boldsymbol{A}^T\boldsymbol{A})^{-1}\boldsymbol{A}^T\boldsymbol{y}$. FMM can then be applied directly, based on this third order polynomial approximation, without any specific reflectance assumption (Lambertian, SEM reflectance function, etc.).

IV. EXPERIMENTS

Both computer simulation and real experiment with SEM imaging were done in order to evaluate the approach.

A. Simulation

Let the image size be 256×256. Let the range of x and y be -3 to $+3$ for the sphere and $-\pi/2$ and $+\pi/2$ for the synthesized test object $z = h \cos x \cos y$, respectively. The radius of the sphere is 2.5 and the height (h) of the test object is 3.5. The synthesized image of the sphere under an oblique light source is shown in Fig. 5(a) with the light source direction of $\alpha = 30$ [deg] and $\beta = 315$ [deg]. FMM is applied to the image and a z distribution is obtained. A NN is constructed to map the "wrong" (p, q) estimated from the z distribution obtained by the FMM to the correct intensity, E, at the corresponding point under the condition of frontal illumination. The target image used to train the NN is shown in Fig. 5(b). The simulation assumes Lambertian reflectance.

NN training was tested with different learning epochs. The spread parameter for the RBF-NN was 0.5 for the distribution of (p, q) and the error goal was set at 10^{-6}. A total of 300 learning epochs was sufficient to train the NN.

The synthesized image of the test object is shown in Fig. 6(a). FMM is applied to this image and (p, q) is estimated from the resulting z distribution. These gradients, (p, q), are input to the NN. The output of the NN is E, as shown in Fig. 6(b). FMM is applied again to the modified image. The recovered result for the test object is shown in Fig. 7(b).

Fig. 7(a) is the recovered shape result for the sphere image itself. As above, FMM is first applied to Fig. 5(a) and (p, q) is estimated from the resulting z distribution. FMM is applied to the modified image, E, to produce Fig. 7(a).

For comparison, results of the Tankus et al. approach [14] are shown in Fig. 8. Their approach decreases the error via iteration and the error status is shown in Table I. It is assumed that the range of values of E is scaled to be between 0 and 1.

TABLE I. ERROR STATUS OF TANKUS *et al.* APPROACH (FOR LAMBERTIAN IMAGE)

	Mean Err.	Max Err.
1 Epoch	0.271	0.581
2 Epoch	0.141	417
3 Epoch	0.098	0.354
4 Epoch	0.079	0.235
5 Epoch	0.063	0.219
6 Epoch	0.055	0.201
7 Epoch	0.061	0.289
8 Epoch	0.078	0.342

With Tankus et al., multiple iterations are required to achieve convergence in shape. Even with convergence, the resulting shape shows some distortion compared to the results of our approach.

With our approach, the mean error and the maximum error for the shape of the recovered sphere were 0.008 and 0.031 respectively. The mean error and the maximum error for the test object were 0.011 and 0.036, respectively. Error for the test object was a little bit larger than for the sphere. A comparison of error between our approach and Tankus et al. is shown in Table II. Compared to Tankus et al., our error was smaller for both objects. In our approach, some points were not learned by the NN owing to self-shadow in the sphere image generated by simulation. Nevertheless, for the test object, intensity modification was correctly done and the resulting z distribution was obtained with higher accuracy.

TABLE II. COMPARISON OF ERROR FOR TEST OBJECT

	Mean Err.	Max Err.
Proposed Approach	0.011	0.036
Approach [14]	0.055	0.201

(a) Input Image (b) Target Image

Fig. 5. Lambertian Sphere

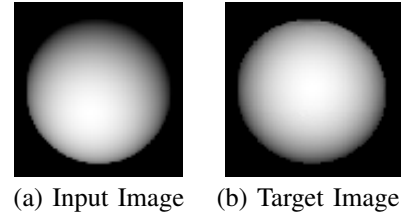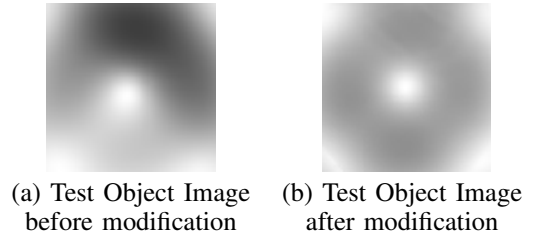(a) Test Object Image before modification (b) Test Object Image after modification

Fig. 6. Test Object Image

B. SEM Sphere Image

A stainless steel sphere with radius 0.5mm was used and the SEM image obtained is shown in Fig. 9(a). FMM was
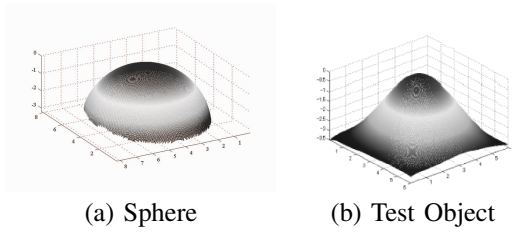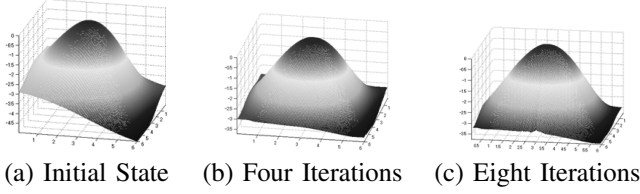
(a) Sphere   (b) Test Object

Fig. 7. Shape Result (Simulation)

(a) Initial State   (b) Four Iterations   (c) Eight Iterations

Fig. 8. Result of Tankus *et al.* Approach (Simulation)

(a) Input Image (before Modification)   (b) Image Used for NN Learning

(c) Contour Image (before Modification)   (d) Contour Image (for NN Learning)

Fig. 10. Sphere Image for NN Learning

applied without further processing and the result is shown in Fig. 9(b). The real sphere SEM image (which corresponds to an oblique light source) and the modified sphere image generated with the affine transformation (which corresponds to frontal illumination) were used to train the NN. Fig. 10(a) repeats the original image of Fig. 9(a). The modified sphere image used to train the NN is shown in Fig. 10(b). The corresponding iso-brightness contour images for Fig. 10(a) and (b) are shown in Fig. 10(c) and (d), respectively.

As in the simulation case, FMM is applied to the real sphere image and (p, q) is estimated from the resulting z distribution. These gradients, (p, q), are input to the NN. FMM is applied again to the modified image to recover the shape for evaluation.

The resulting image after modification with the NN is shown in Fig. 11(a). The result of applying FMM to this image is shown in Fig. 11(b). Analysis confirms that the result from the original image (without modification), shown in Fig. 9(b), has larger error for the original radius of 0.25 [mm]. The result from the modified image, shown in Fig. 11(b), has improved the recovered shape. Unlike in the simulation case, the SEM image of the real sphere has no equivalent to a self-shadow region. This reduces the error when training the NN at every point in real experiments.

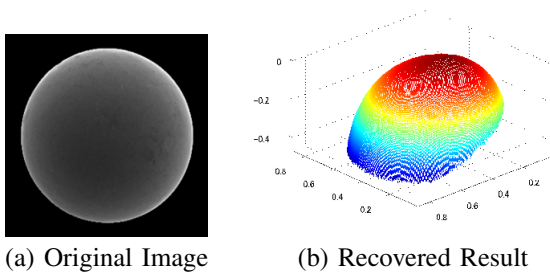(a) Original Image   (b) Recovered Result

Fig. 9. Sphere Result without Modification

Experiment with another test object, a blob of solder, also was done. The original SEM image of the solder blob is shown
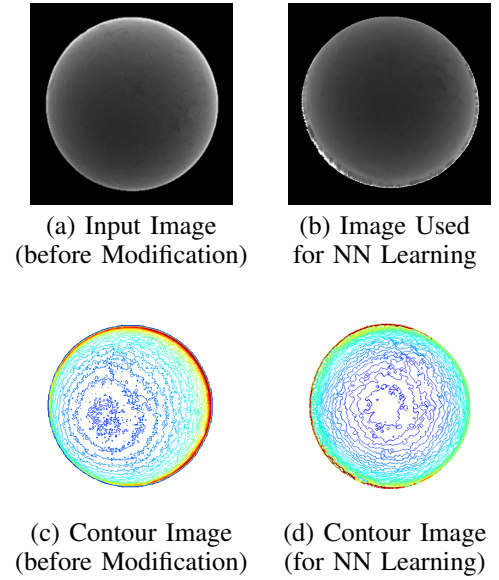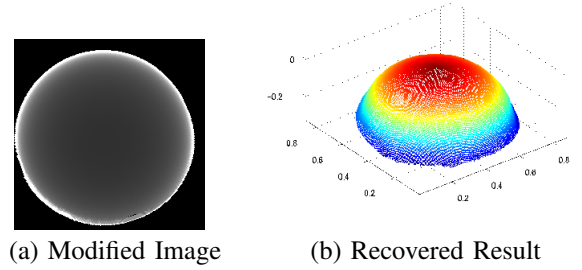

(a) Modified Image   (b) Recovered Result

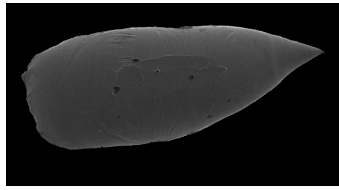Fig. 11. Sphere Result after Modification

in Fig. 12(a). The recovered result, without modification, is shown in Fig. 12(b). The modified image is shown in Fig. 13(a) and the recovered result, with modification, is shown in Fig. 13(b). The convex part of the top point slips out of place in Fig. 13(a) while the corresponding part fits correctly in Fig. 13(b). Quantitative analysis in this case is difficult because the true shape is not known. But, the recovered result of Fig. 13(b) is a qualitatively better result than that of Fig. 12(b).

V. CONCLUSION

This paper described a new approach to recover the 3-D shape from the SEM image of a target object. Assumptions about the alignment of the electron beam with the apparent viewing direction and about the specific functional form for intensity in an SEM image are relaxed. Instead, what is required is obtained from an SEM image of a sphere, used for calibration. Measurements from the calibration sphere are used to train a NN. Once trained, the NN is used to modify the SEM image of the target object so that standard FMM can be applied, without iteration. Experiments show that 3-D shape can be recovered with greater accuracy.

Further topics to explore include application of the approach to test objects with more complex (i.e., convex and concave) shape. The problem to address is that the FMM

generates its solution from a given initial point in depth on the assumption that the surface has a monotonic, convex shape. More complex shapes will require multiple initial points in depth and the ability to segment and to recombine surfaces into distinct convex and concave regions.
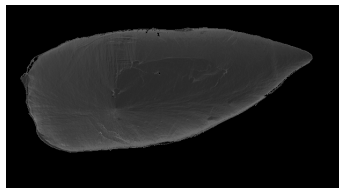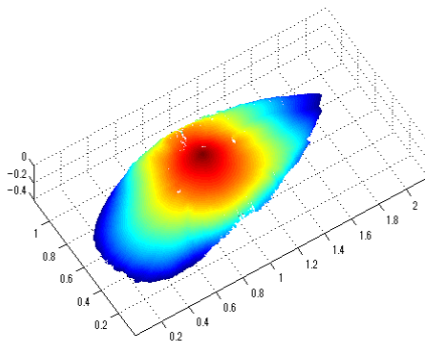

(a) Original Image
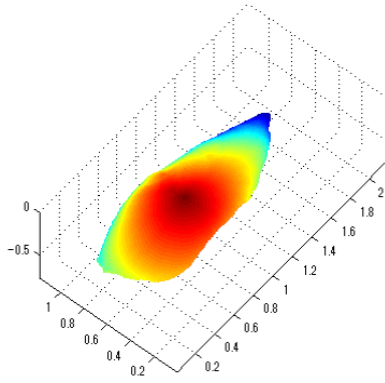
(b) Recovered Result

Fig. 12.   Solder Result without Modification

(a) Modified Image

(b) Recovered Result

Fig. 13.   Solder Result after Modification

REFERENCES

[1] A. P. Pentland, "Linear shape from shading," *International Journal of Computer Vision*, vol. 4, pp. 153–162, 1990.

[2] K. Ikeuchi and B. K. P. Horn, "Numerical shape from shading and occluding boundaries," *Artificial Intelligence*, vol. 17, pp. 141–184, 1981.

[3] A. Laurentini, "How far 3D shapes can be understood from 2D silhouettes," *IEEE Trans. Pattern Anal. Mach. Intell.*, vol. 17, no. 2, pp. 188–195, 1995.

[4] J. Lu and J. J. Little, "Surface reflectance and shape from images using a collinear light source," *International Journal of Computer Vision*, vol. 32, no. 3, pp. 213–240, 1999.

[5] Y. Iwahori, R. J. Woodham, M. Ozaki, H. Tanaka, and N. Ishii, "Neural network based photometric stereo with a nearby rotational moving light source," *IEICE Trans. Info. and Syst.*, vol. E80-D, no. 9, pp. 948–957, 1997.

[6] Y. Iwahori, H. Kawanaka, S. Fukui, and K. Funahashi, "Obtaining shape from scanning electron microscope using Hopfield neural network," *Journal of Intelligent Manufacturing*, vol. 16, no. 6, pp. 715–725, 2005.

[7] J. J. Hopfield and D. W. Tank, "'Neural' computation of decisions in optimization problems," *Biological Cybernetics*, vol. 52, pp. 141–152, 1985.

[8] Y. Iwahori, T. Nakagawa, R. J. Woodham, S. Fukui, and H. Kawanaka "Shape from self-calibration and fast marching method," *19th International Conference on Pattern Recognition (ICPR 2008)*, pp. 1–4, 2008.

[9] H. Ojima, Y. Murakami, H. Otsuka, Y. Sasamoto, L. Zhou, J. Shimizu, and H. Eda, "3D data acquisition and reconstruction from SEM stereo pairs," (in Japanese), *Journal of Japan Society for Precision Engineering*, vol. 75, no. 6, pp. 773–777, 2009.

[10] J. Jiang and S. Sakai, "3-Dimensional measurement of fracture surface using SEM via the combination of stereo matching and integrating secondary electron intensity," (in Japanese), *Journal of Japan Society of Mechanical Engineering*, vol. 68, no. 666, pp. 300–306, 2002.

[11] K. Kamata and K. Deguchi, "3D shape recovery from SEM image using shading information," (in Japanese), *The 21st Sensing Forum, SICE (The Sociery of Instrument and Control Engineers)*, pp. 279–284, 2004.

[12] J. A. Sethian, "A fast marching level set method for monotonically advancing fronts," *Proc. Nat. Acad. Sci.*, vol. 93, no. 4, pp. 1591–1595, 1996.

[13] R. Kimmel and J. A. Sethian, "Optimal algorithm for shape from shading and path planning," *Journal of Mathematical Imaging and Vision*, vol. 14, pp. 237–244, 2001.

[14] A. Tankus, N. Sochen, and Y. Yeshurun, "Shape-from-shading by iterative fast marching for vertical and oblique light sources," in *Geometric Properties for Incomplete Data*, R. Klette *et al.*, Eds., Dordrecht, Netherlands: Springer, pp. 237–258, 2006.

[15] Y. Ding, Y. Iwahori, T. Nakamura, L. He, R. J. Woodham, and H. Itoh, "Neural network implementation of image rendering via self-calibration," *Journal of Advanced Computational Intelligence and Intelligent Informatics*, vol. 14, no. 4, pp. 344–352, 2010.

[16] Y. Iwahori, K. Shibata, H. Kawanaka, K. Funahashi, R. J. Woodham, and Y. Adachi, "Obtaining shape from SEM image using intensity modification via neural network," in *Frontiers in Artificial Intelligence and Applications*, vol. 243, pp. 1778–1787, 2012.

[17] S. Chen, C. F. N. Cowan, and P. M. Grant, "Orthogonal least squares learning algorithm for radial basis function networks," *IEEE Trans. Neural Networks*, vol. 2, no. 2, pp. 302–309, 1991.